Micrometer-Scale Ballistic Transport of Electron Pairs in LaAlO_{3}/SrTiO_{3} Nanowires

Michelle Tomczyk, Guanglei Cheng, Hyungwoo Lee, Shicheng Lu, Anil Annadi, Joshua P. Veazey, Mengchen Huang, Patrick Irvin, Sangwoo Ryu, Chang-Beom Eom, and Jeremy Levy

Phys. Rev. Lett. **117**, 096801 — Published 22 August 2016

DOI: 10.1103/PhysRevLett.117.096801

Micrometer-scale ballistic transport of electron pairs in $LaAlO_3/SrTiO_3$ nanowires

Michelle Tomczyk,[1,2] Guanglei Cheng,[1,2] Hyungwoo Lee,[3] Shicheng Lu,[1,2] Anil Annadi,[1,2] Joshua P. Veazey,[1,*] Mengchen Huang,[1,2] Patrick Irvin,[1,2] Sangwoo Ryu,[3] Chang-Beom Eom,[3] and Jeremy Levy[1,2,†]

[1] *Department of Physics and Astronomy, University of Pittsburgh, Pittsburgh, PA 15260, USA*
[2] *Pittsburgh Quantum Institute, Pittsburgh, PA, 15260 USA*
[3] *Department of Materials Science and Engineering, University of Wisconsin-Madison, Madison, WI 53706, USA*

(Dated: August 10, 2016)

High-mobility complex-oxide heterostructures and nanostructures offer new opportunities for extending the paradigm of quantum transport beyond the realm of traditional III-V or carbon-based materials. Recent quantum transport investigations with $LaAlO_3/SrTiO_3$-based quantum dots have revealed the existence of a strongly correlated phase in which electrons form spin-singlet pairs without becoming superconducting. Here we report evidence for micrometer-scale ballistic transport of electron pairs in quasi-one-dimensional (quasi-1D) $LaAlO_3/SrTiO_3$ nanowire cavities. In the paired phase, Fabry-Perot-like quantum interference is observed, in sync with conductance oscillations observed in the superconducting regime (at zero magnetic field). Above a critical magnetic field B_p, electron pairs unbind and conductance oscillations shift with magnetic field. These experimental observations extend the regime of ballistic electronic transport to strongly correlated phases.

$SrTiO_3$-based heterostructures [1] and nanostructures [2] host a wide range of physical phenomena, including magnetism [3] and superconductivity [4]. In particular, $LaAlO_3/SrTiO_3$ (LAO/STO) heterostructures exhibit strong, tunable spin-orbit coupling [5, 6], a cascade of structural transitions [7], and non-trivial interactions between ferroelastic domain boundaries [8, 9]. LAO/STO-based nanowires possess further surprising behaviors, including *intrinsic* quasi-1D superconductivity [10], and strong electron pairing outside of the superconducting regime [11]. Compared with the 2D superconductor-insulator transition, the nature of correlated electron transport in 1D systems remains largely unexplored. STO-based heterostructures exhibit a relatively short phase coherence, of order ∼100 nm [12, 13]. Exploring the regime where the device dimensions are smaller than the coherence length is challenging; the mobility of devices created by optical or electron-beam lithography generally decreases as the channel width is reduced to sub-micrometer scales [14, 15].

There is growing evidence that scattering lengths, both elastic and inelastic, are greatly enhanced for ultranarrow devices created by conductive atomic force microscope (c-AFM) lithography [2]. With this technique, a voltage-biased c-AFM tip is placed in contact with the LAO surface. Positive voltages applied to the tip locally switch the LAO/STO interface to a conductive state (write), while negative voltages applied to the tip locally restore the LAO/STO interface to an insulating state (erase). The tip can be scanned to draw nanostructures with features as small as 2 nm [16]. It is believed that the tip induces surface protonation and deprotonation [17, 18], effectively modulating the interface conductivity[19] without disrupting the integrity of the interface. Previous transport measurements of ∼10 nm-wide channels at the LAO/STO interface show a nearly two-order-of-magnitude enhancement of room-temperature Hall mobility compared with 2D counterparts [20]. At low temperature, nanowire mobilities exceed 10^4 cm^2/Vs while 2D mobility measurements generally remain an order of magnitude lower [20–23]. Quasi-1D LAO/STO nanowires exhibit conductance values that hover near the single-channel conductance quantum e^2/h, independent of channel length [24]. Additionally, conductance steps have been reported in edge-defined LAO/STO quantum wires [25]. While conductance steps can arise from any point-like constriction [26], and have also been reported in top-gated STO structures that do not possess a 1D geometry [27], such step-like features suggest that LAO/STO nanowires may be able to cleanly resolve individual energy subbands.

Quantum interference experiments can provide useful information about electron scattering. Analogous to photonic interference in an optical Fabry-Perot cavity, multiple reflections of electrons from the endpoints of a nanowire cavity can lead to strong interference effects when the elastic scattering length exceeds the cavity length. This interference requires not only phase coherence but also absence of scattering [28]; many systems with long coherence lengths have much shorter elastic scattering lengths. In ballistic Fabry-Perot cavities, the conductance through the cavity oscillates as a function of the Fermi wavelength, which varies with the chemical potential and is usually controlled by a nearby gate electrode. Only a few material systems have been shown to be capable of supporting micrometer-scale quantum interference: suspended single-wall carbon nanotubes [29], high-mobility graphene structures [30], and III-V semiconductor systems such as high-mobility heterostructures [31] and stacking-fault-free nanowires grown by vapor-liquid-solid techniques [28]. However, these systems often operate in a regime where electron correlations can be

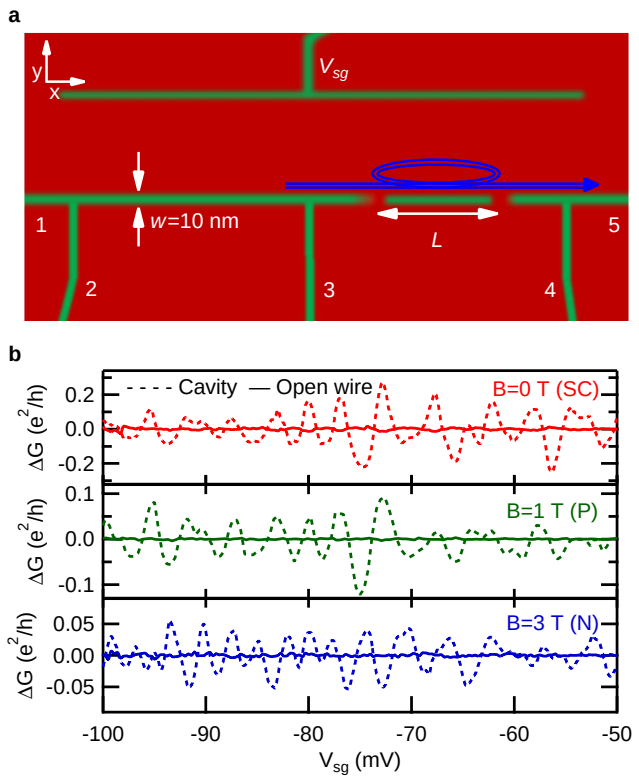

FIG. 1. Device schematic and Fabry-Perot oscillations. (a) Schematic of cavity device defined by two barriers separated by length L. Interference due to coherent scattering in the cavity results in conductance oscillations periodic in Fermi momentum. (b) Background-subtracted zero-bias differential conductance (dI/dV) of the cavity [between voltage leads 3 and 4 in (a)] and the open wire (between leads 2 and 3) in the superconducting (red), paired (green), and normal (blue) phases of Device A clearly reveals large oscillations are only present in the cavity.

neglected; exceptions include Wigner crystal phases, and magnetically and structurally confined one-dimensional systems (i.e., Tomonaga-Luttinger liquids [32]).

In this Letter, we observe evidence of long-range ballistic transport of electron pairs in a complex oxide system. This constitutes a new regime in which strong electronic correlations combine with ballistic electron transport, which is the basis for a remarkable variety of quantum transport phenomena [33], to achieve greater functionality.

To investigate the ballistic nature of transport in LAO/STO nanostructures, quasi-1D Fabry-Perot cavities are created at the LAO/STO interface using c-AFM lithography [2]. To create the geometry shown in Fig. 1(a), first a nanowire of width $w \approx 10$ nm is written, followed by erasure steps to create semitransparent barriers at both ends of the cavity. Devices are transferred to a dilution refrigerator within 5 minutes of writing to minimize decay, and are cooled to a base temperature $T = 50$ mK for transport measurements. Current flows through the main channel containing the two barriers. An applied side gate voltage V_{sg} tunes both the transparency of the barriers and the Fermi level in the cavity. Independent voltage leads enable four-terminal measurements of the cavity conductance, as well as that of an adjoining open nanowire, i.e., without barriers. The differential conductance is extracted numerically from $I-V$ curves measured as a function of V_{sg} and magnetic field. Lock-in measurements are performed at reference frequency $f = 13.46$ Hz and amplitude 100 μV. Cavities of length $L = 0.25 - 4$ μm were studied, and all show qualitatively similar behavior. Additional details of sample growth and fabrication of the nanowire and barriers are described elsewhere (see Supplemental Material [34]).

There are three distinct transport regimes [11] as a function of the applied magnetic field: superconducting (SC), paired (P), and normal (N). At temperatures below $T_c \approx 300$ mK, and for out-of-plane magnetic fields below $B_c = \mu_0 H_{c2} \approx 0.2$ T, the LAO/STO interface exhibits a sharp increase in conductance that is attributed to superconductivity, both for 2D heterostructures [4] and 1D nanowires [10]. The regime $B_c < B < B_p$ has been previously identified as a strongly correlated phase in which electrons exist as spin-singlet pairs without forming a superconducting condensate [11]. At sufficiently large magnetic fields (above $B_p \approx 2 - 5$ T), electrons are unpaired and behave normally.

As a function of V_{sg}, typical differential conductance $G = dI/dV$ measurements of the cavity exhibit quasi-periodic oscillations at zero-bias, i.e., $V_{4T} = 0$ V. The variation in conductance G after subtraction of a slowly-varying background (see Supplemental Materials [34] for details) shows clear oscillations in the cavity, but not in the open wire, in all three phases [Fig. 1(b)]. In the superconducting state, the conductance oscillations correspond to modulation of the critical current [34].

The transconductance dG/dV_{sg} (Fig. 2, left panels), which is computed by numerically differentiating the zero-bias conductance G with respect to side gate, reveals distinct features in the superconducting, paired and normal regimes. The superconducting state is characterized by a sharp conductance peak below $B < B_c$, (Fig. 2, right panels, shaded red); correspondingly, the transconductance exhibits large oscillations. For $B > B_c$, the oscillations decrease in amplitude, yet maintain a definite phase relationship with the superconducting state modulations, confirming that transport continues to be dominated by electron pair states despite the loss of superconducting coherence. This phase relationship is preserved over the magnetic field range $B_c < B < B_p$ (shaded green). A magnetically-induced universal phase shift, which occurs throughout the field range but is hysteretic and not symmetric with field, is subtracted from the data [11, 34]. This global effect does not alter the internal structure of the conductance oscillations. Across $|B| < B_p$, the uni-

versal shift is generally very small compared to the shift at large fields [34], indicating an overall insensitivity to magnetic fields, consistent with the spin-singlet nature of the paired state. For $B > B_p$ (shaded blue), the electron pairs break and the transconductance oscillations split and change markedly with magnetic field.

The observed transconductance oscillations are consistent with Fabry-Perot interference in cavity devices up to 4 μm in length (Fig. 3). Transmission resonances through the cavity occur when the quantum phase associated with round-trip passage is altered by a change in chemical potential or magnetic (Zeeman) interaction. In the equilibrium case [Fig. 3(a),(c),(e), colored lines], in which there is no net bias across the cavity, oscillations appear as a function of the applied side gate voltage, which changes the wavelength of the propagating electron states. In the non-equilibrium regime [Fig. 3(b),(d),(f)], an applied source-drain bias can also change the phase; the result is a characteristic checkerboard pattern similar to what has been reported for other systems such as carbon nanotubes [28, 29]. In Fig. 3(a),(c), and (e), the non-equilibrium linecuts (black) are out-of-phase with the zero-bias oscillations, creating the checkerboard patterns.

Despite all cavity devices exhibiting zero-bias conductance oscillations, full checkerboard patterns extending to finite source-drain bias only appear in small subsets of gate voltage in most devices. For example, the 4 μm cavity exhibits checkerboards for -15 mV $< V_{sg} < 20$ mV in the superconducting and paired phases, and for -75 mV $< V_{sg} < -45$ mV and 10 mV $< V_{sg} < 40$ mV in the normal-state at $B = 7$ T (Fig. 3). Non-equilibrium effects such as heating and the availability of a range of momentum states can dephase transport and damp the oscillations at sufficiently high bias values [Fig. 3(a),(c),(e), black lines]. The preeminence of dips, rather than peaks, has been explained by inter-mode coupling at the scattering centers [29]; the participation of multiple subbands within the cavity increases the likelihood of inter-mode scattering, which can also lead to suppression of coherence signatures at finite bias.

The band structure of the material determines the detailed nature of the observed Fabry-Perot oscillations [46]. Resonant transmission through a cavity of length L is periodic in the Fermi momentum, $k_F = n\pi/L$, so that the period is inversely proportional to length; however, a quadratic relationship between k_F and Fermi energy E_F leads to a resonance period which depends on the effective mass of the energy band, and increases with energy (see Fig. S2) [34]. This is in contrast to the constant periodicity of Fabry Perot oscillations in carbon nanotube systems, which have a linear dispersion [29]. Additionally, bulk STO has three degenerate $3d$ conduction bands with t_{2g} orbital character, and interfacial confinement produces an approximately 50 meV upward shift of the d_{xz} and d_{yz} bands relative to the lighter d_{xy} band

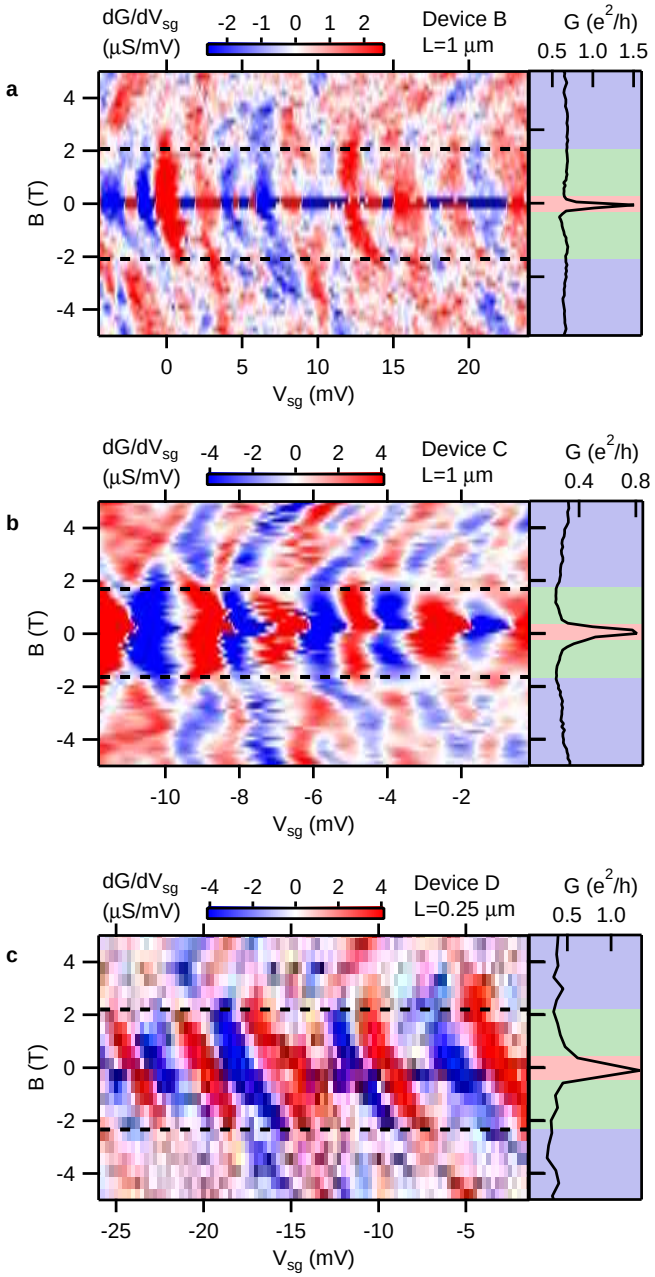

FIG. 2. Magnetic field dependence of conductance oscillations for three devices. Left panels, Transconductance dG/dV_{sg} from a lock-in amplifier measurement of G at small (100 μV) bias versus B and V_{sg}. Alternating red and blue regions correspond to conductance oscillations. Right panels, Linecuts of G versus B, at V_{sg} =0, -2, and 0 mV for (a), (b), and (c) respectively, show a sharp peak attributed to superconductivity at $|B| < B_c \approx 0.2$ T (shaded red), while the conductance in the paired (shaded green) and normal (shaded blue) phases is reduced.

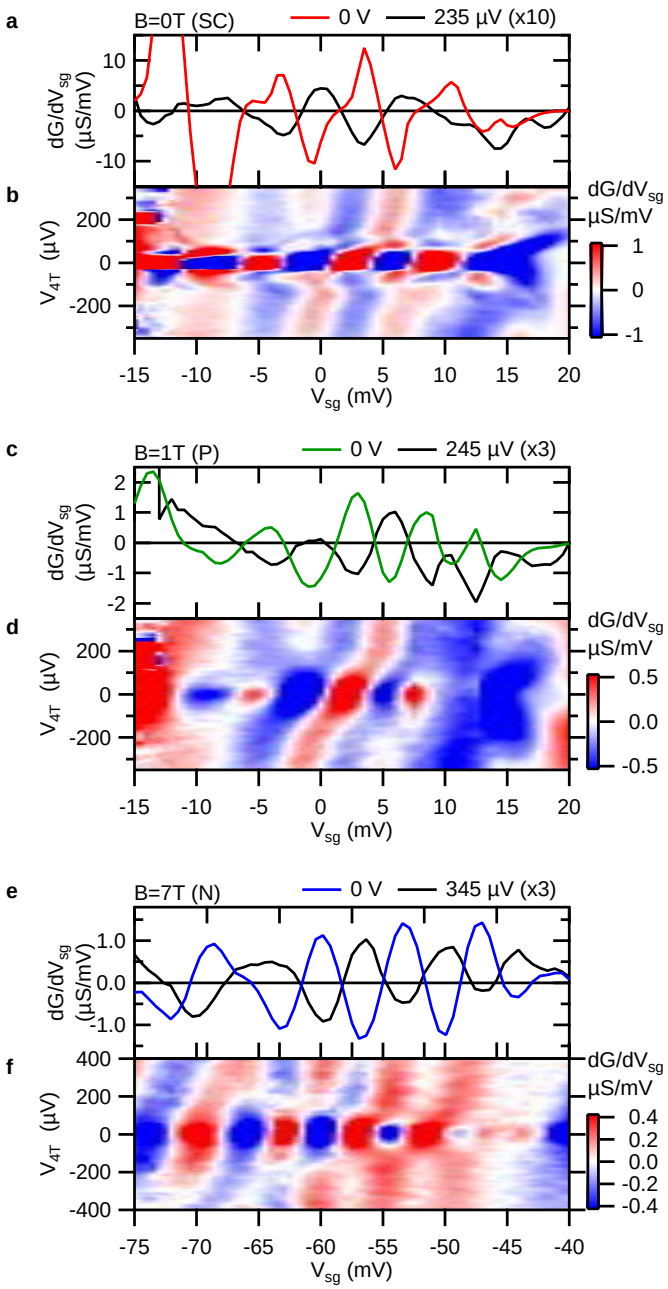

FIG. 3. Fabry-Perot interference signatures at finite bias for an $L = 4\mu$m cavity (Device E). (a), (c), (e), Zero-bias and finite-bias dG/dV_{sg} linecuts as a function of V_{sg} at $B = 0$ T [(a), SC], $B = 1$ T [(c), P], and $B = 7$ T [(e), N]. (b), (d), (f), dG/dV_{sg} vs V_{4T} and V_{sg} in the superconducting phase [(b), $B = 0$ T], paired phase [(d), $B = 1$ T] and normal, unpaired electron phase [(f), $B = 7$ T], showing checkerboard features in each phase.

[47]. The finite width of the quasi-1D nanowire can introduce a manifold of transverse subbands. When new subbands become accessible, abrupt changes in oscillation frequency are expected and observed, and beating between oscillations due to different bands can disrupt a simple checkerboard pattern. These effects can lead to checkerboards appearing in the different subsets mentioned above, and can obscure a direct linear relationship between device length and the interference V_{sg} period. Additionally, inter-mode scattering can affect the Fabry-Perot checkerboards, but is not included in the simple transmission model in Fig. S2.

While conductance oscillations through the cavity are evident for all values of magnetic field explored (up to 9 T), the open wire shows strong suppression of oscillations in all three phases [Fig. 1 (b)]. The root-mean-square amplitude of conductance fluctuations of the open wire is reduced by an order of magnitude compared with the cavity, suggesting that imperfections in the nanowires contribute negligibly to scattering. The pattern of behavior described here, for both cavities and open wires, is consistently observed for all of the 50 cavity devices studied.

Devices with a single manufactured barrier, in which no interference is expected to occur, were also studied, and typical behavior is shown in Supplementary Fig. S8 [34]. Above a conductance value of $\sim e^2/h$, the conductance increases monotonically with increasing gate bias, showing no signs of Fabry-Perot interference. In some devices, Fabry-Perot signatures are observed; however, in each of those devices, the low-V_{sg} regime also shows quantum dot signatures [11]. These signatures are consistent with the existence of a second, unintentional potential barrier along the nanowire that creates a cavity and associated interference patterns.

While systems which support Fabry-Perot interference are expected to act as quantum dots when tuned to a tunneling regime, not all 1D quantum dot systems can exhibit Fabry-Perot interference [48]. Resonant tunneling observed in LAO/STO nanowire-based quantum dots at low V_{sg} suggests that extended coherent states exist [11], but does not rule out disorder, which randomizes carrier paths in the transport regime at high V_{sg}. In contrast, Fabry-Perot interference as described here demonstrates micrometer-scale elastic scattering lengths in these nanowire cavities. Interestingly, such clean 1D transport differs from behavior reported in 2D devices. However, local probes have revealed the existence of narrow channel flow along ferroelastic domain boundaries [8, 9], so understanding the distinctive transport in quasi-1D structures is possibly relevant for transport measurements of the 2D LAO/STO interface.

Specifically, the observation of Fabry-Perot interference in the paired regime provides evidence for ballistic transport of electron pairs in the quasi-1D LAO/STO nanowire system. This result is in sharp contrast to

Cooper pair insulators, in which electron pairs surviving outside of the superconducting state are localized [49]. Metallic Bose phases have been observed in both optical lattice [50] and solid state [49] systems, but even in clean superconductors where the mean free path is longer than the superconducting coherence length, the mean free path is only on the order of 10 nm [51]. Additionally, these metallic Bose phases always appear below the upper critical field for superconductivity in their systems. The results observed here in LAO/STO nanowires are distinct due to both the ballistic nature of transport of the uncondensed electron pairs, and the persistence of this ballistic pair state well above the upper critical field for superconductivity in LAO/STO.

Coherent, ballistic transport can be associated with delocalization of the electron wavefunction. For the case of ballistic electron pairs, this description is inadequate since it does not describe the strong correlations leading to the formation of composite bosons. Furthermore, what happens when this delocalization length greatly exceeds the superconducting coherence length? In LAO/STO, the superconducting coherence length is $\sim$ 100 nm [4], much shorter than the micrometer-scale ballistic transport of electrons and electron pairs. Can competition between superconductivity and delocalization alter or suppress the superconducting state in these nanowires? A theoretical framework is necessary for answering the questions raised by the ballistic transport of electron pairs.

Long-range coherent and ballistic transport in a strongly-correlated electronic phase suggest LAO/STO nanowires are promising candidates for studying the rich theoretical predictions for one-dimensional transport [52], including charge/spin separation [32]. These results, along with the reconfigurable nature of this interface system, indicate further applications of this system as a platform for quantum information and simulation by using these ballistic nanowires as quantum buses for both electrons and electron pairs with modifiable correlations.

This work was supported by ARO MURI W911NF-08-1-0317 (J.L.), AFOSR MURI FA9550-10-1-0524 (C.B.E., J.L.), FA9550-12-1-0342 (C.B.E.), and FA9550-15-1-0334 (C.B.E.), and grants from the National Science Foundation DMR-1104191 (J.L.), DMR-1124131 (C.B.E., J.L.) and DMR-1234096 (C.B.E.).

* Present Address: Department of Physics, Grand Valley State University, Allendale, MI 49401
† Corresponding Author: jlevy@pitt.edu

[1] A. Ohtomo and H. Y. Hwang, Nature **427**, 423 (2004).
[2] C. Cen, S. Thiel, G. Hammerl, C. W. Schneider, K. E. Andersen, C. S. Hellberg, J. Mannhart, and J. Levy, Nature Materials **7**, 298 (2008).
[3] A. Brinkman, M. Huijben, M. Van Zalk, J. Huijben, U. Zeitler, J. C. Maan, W. G. Van der Wiel, G. Rijnders, D. H. A. Blank, and H. Hilgenkamp, Nature Materials **6**, 493 (2007).
[4] N. Reyren, S. Thiel, A. D. Caviglia, L. F. Kourkoutis, G. Hammerl, C. Richter, C. W. Schneider, T. Kopp, A. S. Ruetschi, D. Jaccard, M. Gabay, D. A. Muller, J. M. Triscone, and J. Mannhart, Science **317**, 1196 (2007).
[5] M. Ben Shalom, M. Sachs, D. Rakhmilevitch, A. Palevski, and Y. Dagan, Physical Review Letters **104**, 126802 (2010).
[6] A. D. Caviglia, M. Gabay, S. Gariglio, N. Reyren, C. Cancellieri, and J. M. Triscone, Physical Review Letters **104**, 126803 (2010).
[7] K. A. Muller and H. Burkard, Physical Review B **19**, 3593 (1979).
[8] B. Kalisky, E. M. Spanton, H. Noad, J. R. Kirtley, K. C. Nowack, C. Bell, H. K. Sato, M. Hosoda, Y. Xie, Y. Hikita, C. Woltmann, G. Pfanzelt, R. Jany, C. Richter, H. Y. Hwang, J. Mannhart, and K. A. Moler, Nature Materials **12**, 1091 (2013).
[9] M. Honig, J. A. Sulpizio, J. Drori, A. Joshua, E. Zeldov, and S. Ilani, Nature Materials **12**, 1112 (2013).
[10] J. P. Veazey, G. L. Cheng, P. Irvin, C. Cen, D. F. Bogorin, F. Bi, M. C. Huang, C. W. Bark, S. Ryu, K. H. Cho, C. B. Eom, and J. Levy, Nanotechnology **24**, 8 (2013).
[11] G. L. Cheng, M. Tomczyk, S. C. Lu, J. P. Veazey, M. C. Huang, P. Irvin, S. Ryu, H. Lee, C. B. Eom, C. S. Hellberg, and J. Levy, Nature **521**, 196 (2015).
[12] D. Rakhmilevitch, M. Ben Shalom, M. Eshkol, A. Tsukernik, A. Palevski, and Y. Dagan, Physical Review B **82**, 235119 (2010).
[13] X. Lin, Z. Zhu, B. Fauque, and K. Behnia, Physical Review X **3**, 021002 (2013).
[14] C. W. Schneider, S. Thiel, G. Hammerl, C. Richter, and J. Mannhart, Applied Physics Letters **89**, 122101 (2006).
[15] J. W. Chang, J. Song, J. S. Lee, H. Noh, S. K. Seung, L. Baasandorj, S. G. Lee, Y. J. Doh, and J. Kim, Applied Physics Express **6** (2013), Artn 085201 Doi 10.7567/Apex.6.085201.
[16] C. Cen, S. Thiel, J. Mannhart, and J. Levy, Science **323**, 1026 (2009).
[17] F. Bi, D. F. Bogorin, C. Cen, C. W. Bark, J. W. Park, C. B. Eom, and J. Levy, Applied Physics Letters **97**, 173110 (2010).
[18] K. A. Brown, S. He, D. J. Eichelsdoerfer, M. Huang, I. Levy, H. Lee, S. Ryu, P. Irvin, J. Mendez-Arroyo, C.-B. Eom, C. A. Mirkin, and J. Levy, Nat Commun **7** (2016), 10.1038/ncomms10681.
[19] R. Dingle, H. L. Stormer, A. C. Gossard, and W. Wiegmann, Applied Physics Letters **33**, 665 (1978).
[20] P. Irvin, J. P. Veazey, G. L. Cheng, S. C. Lu, C. W. Bark, S. Ryu, C. B. Eom, and J. Levy, Nano Letters **13**, 364 (2013).
[21] A. D. Caviglia, S. Gariglio, C. Cancellieri, B. Sacepe, A. Fete, N. Reyren, M. Gabay, A. F. Morpurgo, and J. M. Triscone,

Physical Review Letters **105**, 236802 (2010).
[22] D. Stornaiuolo, S. Gariglio, N. J. G. Couto, A. Fte, A. D. Caviglia, G. Seyfarth, D. Jaccard, A. F. Morpurgo, and J.-M. Triscone, Applied Physics Letters **101**, 222601 (2012).
[23] N. Banerjee, M. Huijben, G. Koster, and G. Rijnders, Applied Physics Letters **100** (2012), Artn 041601 10.1063/1.3679379.
[24] G. Cheng, J. P. Veazey, P. Irvin, C. Cen, D. F. Bogorin, F. Bi, M. Huang, S. Lu, C.-W. Bark, S. Ryu, K.-H. Cho, C.-B. Eom, and J. Levy, Physical Review X **3**, 011021 (2013).
[25] A. Ron and Y. Dagan, Physical Review Letters **112**, 136801 (2014).
[26] B. J. van Wees, H. van Houten, C. W. J. Beenakker, J. G. Williamson, L. P. Kouwenhoven, D. van der Marel, and C. T. Foxon, Physical Review Letters **60**, 848 (1988).
[27] P. Gallagher, M. Lee, J. R. Williams, and D. Goldhaber-Gordon, Nature Physics **10**, 748 (2014).
[28] A. V. Kretinin, R. Popovitz-Biro, D. Mahalu, and H. Shtrikman, Nano Letters **10**, 3439 (2010).
[29] W. J. Liang, M. Bockrath, D. Bozovic, J. H. Hafner, M. Tinkham, and H. Park, Nature **411**, 665 (2001).
[30] F. Miao, S. Wijeratne, Y. Zhang, U. C. Coskun, W. Bao, and C. N. Lau, Science **317**, 1530 (2007).
[31] J. A. Simmons, D. C. Tsui, and G. Weimann, Surface Science **196**, 81 (1988).
[32] F. D. M. Haldane, Journal of Physics C-Solid State Physics **14**, 2585 (1981).
[33] Y. V. Nazarov and Y. M. Blanter, *Quantum Transport: Introduction to Nanoscience* (Cambridge University Press, Cambridge, UK ; New York, 2009).
[34] See the Supplemental Material, which includes Refs. [35-45], for details on sample growth, nanolithography, modeling of Fabry-Perot interference, background-subtraction calculations, calculations of critical current, and single barrier devices.
[35] J. W. Park, D. F. Bogorin, C. Cen, D. A. Felker, Y. Zhang, C. T. Nelson, C. W. Bark, C. M. Folkman, X. Q. Pan, M. S. Rzchowski, J. Levy, and C. B. Eom, Nature Communications **1**, 94 (2010).
[36] C. W. Bark, D. A. Felker, Y. Wang, Y. Zhang, H. W. Jang, C. M. Folkman, J. W. Park, S. H. Baek, H. Zhou, D. D. Fong, X. Q. Pan, E. Y. Tsymbal, M. S. Rzchowski, and C. B. Eom, Proceedings of the National Academy of Sciences of the United States of America **108**, 4720 (2011).
[37] C. W. Bark, P. Sharma, Y. Wang, S. H. Baek, S. Lee, S. Ryu, C. M. Folkman, T. R. Paudel, A. Kumar, S. V. Kalinin, A. Sokolov, E. Y. Tsymbal, M. S. Rzchowski, A. Gruverman, and C. B. Eom, Nano Letters **12**, 1765 (2012).
[38] G. L. Cheng, P. F. Siles, F. Bi, C. Cen, D. F. Bogorin, C. W. Bark, C. M. Folkman, J. W. Park, C. B. Eom, G. Medeiros-Ribeiro, and J. Levy, Nature Nanotechnology **6**, 343 (2011).
[39] A. Levy, F. Bi, M. Huang, S. Lu, M. Tomczyk, G. Cheng, P. Irvin, and J. Levy, Journal of Visualized Experiments **89**, e51886 (2014).
[40] S. Thiel, G. Hammerl, A. Schmehl, C. W. Schneider, and J. Mannhart, Science **313**, 1942 (2006).
[41] J. N. L. Connor, Molecular Physics **15**, 37 (1968).
[42] A. F. Santander-Syro, O. Copie, T. Kondo, F. Fortuna, S. Pailhes, R. Weht, X. G. Qiu, F. Bertran, A. Nicolaou, A. Taleb-Ibrahimi, P. Le Fevre, G. Herranz, M. Bibes, N. Reyren, Y. Apertet, P. Lecoeur, A. Barthelemy, and M. J. Rozenberg, Nature **469**, 189 (2011).
[43] G. Kirczenow, Physical Review B **39**, 10452 (1989).
[44] J. P. Veazey, G. Cheng, S. Lu, M. Tomczyk, F. Bi, M. Huang, S. Ryu, C. W. Bark, K. H. Cho, C. B. Eom, P. Irvin, and J. Levy, Europhysics Letters **103**, 57001 (2013).
[45] P. Jarillo-Herrero, J. A. van Dam, and L. P. Kouwenhoven, Nature **439**, 953 (2006).
[46] Q. Wang, N. Carlsson, I. Maximov, P. Omling, L. Samuelson, W. Seifert, W. D. Sheng, I. Shorubalko, and H. Q. Xu, Applied Physics Letters **76**, 2274 (2000).
[47] M. Salluzzo, J. C. Cezar, N. B. Brookes, V. Bisogni, G. M. De Luca, C. Richter, S. Thiel, J. Mannhart, M. Huijben, A. Brinkman, G. Rijnders, and G. Ghiringhelli, Physical Review Letters **102**, 166804 (2009).
[48] M. R. Buitelaar, A. Bachtold, T. Nussbaumer, M. Iqbal, and C. Schonenberger, Physical Review Letters **88**, 156801 (2002).
[49] P. Phillips and D. Dalidovich, Science **302**, 243 (2003).
[50] B. Deissler, M. Zaccanti, G. Roati, C. D'Errico, M. Fattori, M. Modugno, G. Modugno, and M. Inguscio, Nature Physics **6**, 354 (2010).
[51] A. W. Tsen, B. Hunt, Y. D. Kim, Z. J. Yuan, S. Jia, R. J. Cava, J. Hone, P. Kim, C. R. Dean, and A. N. Pasupathy, Nature Physics **12**, 208 (2016).
[52] T. Giamarchi, Chemical Reviews **104**, 5037 (2004).